

Abstract.—The objective of our study was to model the performance of an airborne lidar survey system for northern anchovy in terms of survey accuracy and precision. Our analyses indicated that swath width would have little or no effect on the probability that at least one fish school would be encountered. In typical coastal waters off California (attenuation coefficient=0.1/m), about half of the schools were detected by the lidar during the day and about 64% during the night. A greater proportion of schools were detected during the night because anchovy have a shallow vertical distribution, whereas in the day, schools may extend down to 155 m; schools below about 40 m depth were not detectable to the laser. Although schools tended to be more diffuse during the night than during the day, even the very diffuse schools of anchovy (0.5 fish/m³) were detectable at night throughout the upper 20 m of the water column with a lidar. With a substantial increase in instrument and survey costs, it would be possible to increase the equivalent laser-pulsed power by a factor of 10 over that of the “off-the-shelf system,” as used in our model. Such a change would increase the maximum detection depth of the lidar system by about 10 m but would have a negligible effect on the probability of detecting schools during the day owing to the skewed vertical distribution of anchovy schools. More effective approaches for improving the accuracy and precision of potential lidar surveys for fisheries would be to improve school detection algorithms and to develop a lidar survey model based on line transect theory to obtain an unbiased estimate of abundance. To produce an accurate reconstruction of the average vertical distribution of schools for a particular season and region, a synthesis of acoustic and lidar surveys of school distribution is required.

Manuscript accepted 18 November 1999.
Fish. Bull. 98:264–282 (2000).

Modeling statistical performance of an airborne lidar survey system for anchovy

Nancy C. H. Lo

John R. Hunter

Southwest Fisheries Science Center
National Marine Fisheries Service, NOAA
P.O. Box 271, La Jolla, California 92038
E-mail address (for N.C.H. Lo): Nancy.Lo@noaa.gov

James H. Churnside

Ocean Remote Sensing Division
Environmental Technology Laboratory
325 Broadway, Boulder, Colorado 80303

Airborne lidar surveys are an attractive alternative to the methods presently used in fishery-independent surveys of epipelagic fishes (Hunter and Churnside¹). They would cost much less per survey mile than ship-based methods (acoustic-trawl, ichthyoplankton), and the survey would extend to greater depths than present aerial methods. A lidar, (li[ght] d[etecting] and r[anging]) system, in its most basic form, produces short pulses of laser light that pass through the water surface and reflect off fish and particles in the water; a receiver measures the returning reflected pulse; the strength of the returning pulse separates fish targets from small particles, and the elapsed time from start to return of pulses indicates the range (depth below the surface) of the target. The application of lidar technology to fishery surveys is still in its infancy. Fish schools have been detected with a variety of lidar systems (Churnside and Hunter, 1996), but schools have never been systematically studied with lidar, nor has existing lidar technology been adapted to fish-survey needs; formal fish surveys have never been conducted.

A lidar survey system for fishery-independent monitoring of epipelagic fish stocks is being developed jointly

by two laboratories of the National Oceanic Atmospheric Administration (NOAA): Environmental Technical Laboratory, Boulder, CO; and Southwest Fisheries Science Center, La Jolla, CA. The approach is to combine evaluations of prototype instruments at sea with modeling of survey performance to develop an optimal lidar survey system. The goal is to develop a system that will deliver the greatest statistical precision for the lowest survey cost, while minimizing potential biases. In our study, we modeled a lidar survey with the objective of evaluating how instruments would affect survey precision or accuracy. Two classes of instrument design were considered, those affecting fish schools in the horizontal plane (swath width) and those affecting the detection of fish schools in the vertical plane (depth-specific detection). We also analyzed a trade-off between swath width and penetration depth, which is analogous to changing from a visual-based aerial survey (wide swath, shallow penetration) to a lidar-based

¹ Hunter, J. R., and J. H. Churnside, eds. 1995. Airborne fishery assessment technology—a NOAA workshop report. SWFSC Admin. Rep. LJ-95-02, 33 p. Southwest Fish. Sci. Ctr., NMFS, NOAA, P.O. Box 271, La Jolla, CA 92038.

aerial survey (narrow swath, deeper penetration). We discuss each.

Precision of an airborne lidar survey will depend upon the number of transects flown and the probability of encountering schools along them. The width of the transect lines (swath width), may affect the probability of encountering schools and therefore could be one of the few factors affecting precision that involve instrument design. Swath width could be increased in a variety of ways (flying higher, scanning or optically expanding the laser beam), but such changes are accompanied by disadvantages (loss in penetration depth, reduced resolution, increased instrument cost and weight). In our study, we modeled how the width of the swath (width of transect line) cut by the survey instrument affects the probability of encountering fish schools, and therefore the precision of the survey estimate, assuming fish are uniformly distributed in the water column.

The accuracy of a biomass survey depends on the extent to which the entire stock is vulnerable to the counting technique and on the variability in size of the uncounted fraction (Gunderson, 1993). The key issue for accuracy of a lidar survey is the vulnerability of a stock to being counted in the vertical plane. Depth-specific detection by a lidar depends upon laser power, sensitivity of the detection system, the rate of exponential decay of the laser pulse with water depth, the way the fish-detection function of the instrument changes with signal attenuation, fish size and reflectivity, school packing density, and, of course, the vertical distribution of the fish. Using a set of models and taking into account many of these variables, we evaluated the effect of instrument and survey design on the accuracy of an aerial lidar survey for measuring fish abundance. We considered how variations in laser power, school size, diel changes in vertical distribution of schools and school packing density (number of fish per m^3) would affect the accuracy of the survey. We also used these models to estimate the maximum depth at which schools might be detected by a single lidar pulse. For our study, we chose to use anchovy because more data exist on anchovy schools than most other species. Lo et al.² have, however, recently applied the same models to sardine and herring schools.

Materials and methods

We used various models to evaluate the potential effects of instruments on survey design. To evaluate

how swath width may affect survey accuracy, simulation runs were used for a school-group encounter model. To evaluate the relation between laser power and maximum detection depth for fish schools, we computed the probability of detecting schools as a function of the signal-to-noise-ratio and estimated laser power and the laser attenuation coefficient. School parameters, size, distribution and density, and survey area ($46,204 \text{ km}^2=333 \text{ km (180 nmi)} \times 138.75 \text{ km (75 nmi)}$) were taken from acoustic surveys of northern anchovy in the Southern California Bight (Mais, 1974; Fiedler, 1978; Smith, 1981; MacCall³). For daytime profiles, vertical distributions of schools were based on northern anchovy off California (Holliday and Larsen, 1979); for nighttime profiles we used the distribution of early stage anchovy eggs (Pommeranz and Moser, 1987) and acoustic data for anchoveta off Peru (Castillo Valderrama, 1995). Signal-to-noise ratio was based on information on packing density of schools provided by Aoki and Inagaki (1988) and Graves (1977).

Many pelagic fish schools form distinct aggregations or school groups (Cram and Hampton, 1976; Fiedler, 1978). The area of an anchovy school (expressed by school diameter in our study) is highly variable, as are the size and number of schools within a school group. Because of this complexity, simulations were used to compute the probability of encountering anchovy schools in a survey area (Fiedler, 1978).

In the simulation, school groups were randomly assigned in the survey area. The sizes of the anchovy schools within a group were generated from the frequency distribution of the diameters of northern anchovy schools in the Southern California Bight (Fiedler, 1978; Smith, 1981; Table 1). The number of anchovy schools within an anchovy school group was generated from the area occupied by the group and the density of schools. Both the diameters of school groups and the density of schools within a school group were assumed to follow the lognormal distributions measured for anchovy in the Southern California Bight (Fiedler, 1978; Smith, 1981) (Fig. 1). Simulations were used to compute the encounter probability (p_Y) for various swath widths (Y).

The locations of school groups were randomly allocated in north–south (n–s) and east–west (e–w) directions. When school groups overlapped (intersected) in the north–south directions, they were combined as a “single” school group for computing the encoun-

² Lo, N. C. H., J. R. Hunter, and J. H. Churnside. 1999. Modeling properties of airborne lidar surveys for epipelagic fish. Admin. Rep. LJ-99-01. Southwest Fish. Sci. Ctr. NMFS, NOAA. P.O. Box 271, La Jolla, CA 92037.

³ MacCall, A. 1975. Anchovy population survey simulation: a report of CalCOFI Anchovy Workshop Group on methods of estimating anchovy abundance, July 21–22, 1975, Contribution 4, 9 p. Marine Life Research Group, Scripps Institution of Oceanography, 9500 Gilman Drive, La Jolla, CA 92037-0227.

Table 1

The frequency distribution of school sizes of anchovy in the Los Angeles Bight based on sonar mapping conducted by the California Department of Fish and Game (Mais, 1974; Smith, 1981).

School diameter (m)	Frequency	Sample proportions
10	9906	0.4338
30	9002	0.3942
50	1822	0.0798
70	706	0.0309
90	824	0.0361
110	178	0.0078
130	217	0.0095
150	50	0.0022
170	40	0.0018
190	51	0.0022
210	19	0.0008
230	7	0.0003
250	3	0.0001
270	1	<0.0001
290	2	0.0001
310	1	<0.0001
330	3	0.0001
350	0	0
370	0	0
390	2	0.0001

ter probability. Only the north–south direction was relevant because the transect was run from east to west. Similarly, schools were randomly allocated within a school group and when schools overlapped in the north–south direction, they were combined as a “single” school for computing purposes. This process continued until all schools were separated in the north–south direction and termed “disjoint” schools. The distance (gaps) between disjoint schools in the north–south direction were summed for each school group and later summed for all fish groups. The sum of n–s gaps within school groups was termed “total gap within.” Similarly, a “total gap between” (disjoint school groups) was also computed. Both “total gap within” and “total gap between” were used to compute the encounter probability (p_y) (the probability that at least one fish school is detected):

$$p_y = 1 - (\text{total gap within} + \text{total gap between})/L$$

or

$$p_y = 1 - \frac{\sum_i^n \sum_j^{J_i-1} (g_{ij} - y) + \sum_i^{n-1} (G_i - y) + E}{L}, \quad (1)$$

where y = the swath width in meter;

g_I = the gap length between j^{th} and $j+1^{\text{th}}$ disjoint school within a school group and the quantity of $g_{ij} - y$ is set to zero if g_{ij} is less than y ;

G_I = the gap length between i^{th} and $i+1^{\text{th}}$ disjoint school groups and $G_i - y$ is set to zero if G_i is less than y ;

E = the distance between the north and south end of the survey area and their nearest anchovy schools;

N = number of school groups disjoint in the north–south direction; and

L = 333 km (180 nautical miles [nmi]) which is about the length of the coastline along the Southern California Bight.

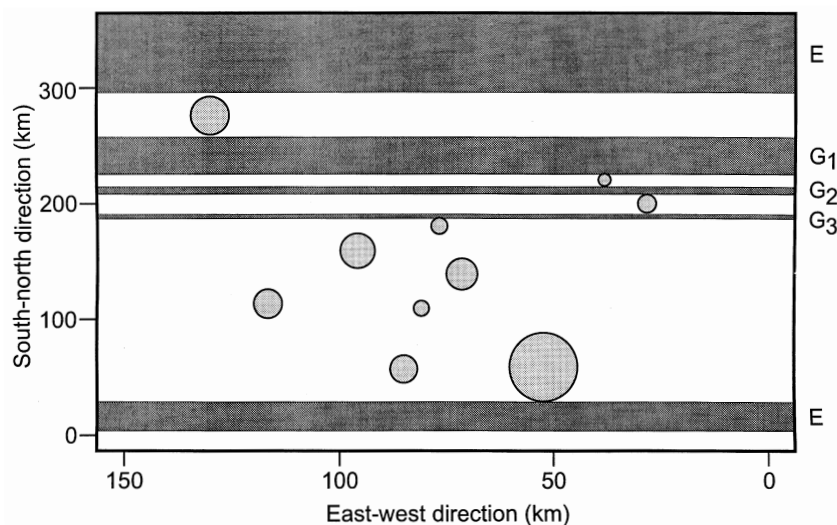


Figure 1

A spatial distribution of school groups from one simulation run. Circles indicate areas covered by school groups for a population of 80,000 schools. This graph was generated from lognormal distributions with mean = 3.91 and variance = 0.51 for school density (number of schools/nmi²) and from lognormal distribution with mean = 2.319 and variance = 0.676 for diameter (nmi) of school group (nmi was later converted to km). G1, G2, G3, and E are the gaps used to compute the encounter probability (Eq. 1).

Smith (1981) reported that the diameter (nmi) of a school group followed a lognormal distribution and had a logarithmic mean of 2.319 and a logarithmic variance

of 0.676, and that the density of fish schools/nmi² in a school group had a logarithmic mean of 3.91 and a logarithmic variance of 0.51 based on data from MacCall.³ The number of schools within a school group is the product of the area of the school group and the density of schools within. Thus, the mean number of schools was 10,274⁴ in a school group (Table 2). The diameter of anchovy schools was generated from the frequency distribution of the diameters of anchovy fish schools in the Southern California Bight (Table 1).

On average, there were 150,000 anchovy schools in the Southern California Bight in the 1970s (Mais, 1974). In recent years, the population has decreased to one fifth of that level (Jacobson et al., 1994). In the simulation, we constructed populations comprising 80,000, 32,000, and 16,000 schools with an average biomass of 12 metric tons (t). At each population level of anchovy, we simulated school groups for nine combinations of three school diameters and three school densities, each with a multiplier of 0.5, 1, and 1.5 applied to both mean and standard deviation of $\ln(\text{school diameters})$ and of $\ln(\text{density of schools})$ respectively (Table 2). For example, for a population of 32,000 schools, a multiplier of 0.5 applied to both mean and standard deviation of $\ln(\text{diameter})$ (an area of 9.45 nmi² or 32.34 km²) for a school group,⁵ and a multiplier of 1.5 applied to the mean and standard deviation of $\ln(\text{density})$ (625 schools /nmi² or 182 schools/km²),⁶ would yield an average number of 5914 schools per school group and an average of six school groups (32,000/5914) (Table 2). This population was denoted as 32,000 (0.5,1.5). The encounter probabilities for seven swath widths (1, 10, 50, 200, 500, 900, and 1600 m for a total of 63 (3 × 3 × 7) sets of scenarios) were simulated (in computation, numeral 1 was used to represent diameters less than or equal to 1 m). For each of the three populations, 500 iterations were run for each of 63 sets. The mean of the encounter probabilities from 500 runs was used to estimate the mean encounter probability.

For multiple swaths (n), the probability ($p_{y,n}$) that at least one of the swaths intercepts schools is computed as

$$p_{y,n} = 1 - (1 - p_y)^n, \tag{2}$$

where p_y is computed from Equation 1.

⁴ The mean diameter is 14.25 nmi = $\exp(2.319+0.676/2)$ and the mean density of fish schools is 64.39 schools/nmi² = $\exp(3.91+0.51/2)$, the mean number of fish schools in a school group = $(14.25/2)^2 \times 64.39 = 10,274$.

⁵ $[\exp(2.319 \times 0.5 + 0.676 \times 0.5 \times 0.5/2)]^2 \times 3.1416 = 9.45 \text{ nmi}^2$.

⁶ $\exp(3.91 \times 1.5 + 0.51 \times 1.5 \times 1.5/2) = 625.62 \text{ schools/nmi}^2$.

Table 2

The average number of school groups for three population sizes and the average number of schools per school group for combinations of different multipliers for the school densities and the school diameters (see text).

Multipliers for diameter of school groups	Multipliers for school density		
	0.5	1.0	1.5
Average number of school groups for three population sizes:			
Population: 16000 schools			
0.5	224.79	26.28	2.71
1.0	13.32	1.56	0.16
1.5	0.56	0.07	0.01
Population: 32000 schools			
0.5	449.58	52.56	5.41
1.0	26.64	3.11	0.32
1.5	1.13	0.13	0.01
Population: 80000 schools			
0.5	1123.94	131.41	13.53
1.0	66.59	7.79	0.80
1.5	2.81	0.33	0.03
Average number of schools per school group			
0.5	71.18	608.77	5914.65
1.0	1201.33	10274.66	99826.39
1.5	28429.65	243150.98	2362398.24

Estimating the number of swaths needed in a survey

Typically, the optimal sample size for a survey is computed by minimizing the variance of the estimate subject to a fixed cost. Because this information was not available, we defined a desirable sample size in terms of the minimum number of transect lines or swaths needed to guarantee at least one positive sighting at an acceptable probability. Therefore, from p_y in Equation 1, one can compute the number of swaths (n) needed for a desired value of $p_{y,n}$ by using

$$n = \frac{\ln(1 - p_{y,n})}{\ln(1 - p_y)}. \tag{3}$$

Probability of detecting fish by depth with signal-to-noise ratios (SNR)

The signal level of a lidar system decays exponentially with depth. The decaying signal of a single pulse can be expressed by the equation

$$S(z) = S_0 \frac{\beta_w(z) + \beta_f(z)}{\beta_0} \exp(-2\alpha z), \tag{4}$$

where z = depth in meters;
 S_0 = the signal level at the surface;
 β_w = the clear-water backscatter coefficient;
 β_f = the backscatter coefficient of a school of fish;
 β_0 = the backscatter coefficient at the surface; and
 α = the lidar attenuation coefficient.

The backscatter coefficients, β , have units of 1/m and represent the fraction of the energy that would be scattered upward by a 1-m layer of either clear water or fish. By clear water we mean natural sea water with its attendant load of yellow substance, plankton, silt, etc., but without fish. The lidar attenuation coefficient is related to the absorption and scattering coefficients of the water, in a way that is not completely understood, but depends on the field of view of the lidar. In an operational system, this parameter can be obtained directly from the lidar data. A very narrowly collimated system (defined as one where the field of view is much smaller than the average scattering angle in the water and much smaller than the ratio of the beam attenuation coefficient to the lidar height) will have an attenuation that is very close to the sum of the absorption and scattering. A wide field of view collects multiple scattered photons, and the attenuation is closer to the absorption coefficient.

The noise in a lidar system can come from several different processes. One of these is likely to predominate in any particular set of circumstances. One source is thermal noise in the receiver. This is an additive noise that is independent of the signal level. It is Gaussian with a zero mean. Another source of noise is the shot noise from the sum of the signal current, background-light-generated current, and detector dark current. This is a Poisson process that depends on the total detector current. However, except for very low illumination levels, the Poisson distribution is nearly Gaussian, and we made this approximation. Also, we noted that if the signal from the fish school is very large, the detection probability is nearly unity, and accurate modeling of the noise distribution is not critical. If the fish signal is small, the shot-noise variance will be very nearly the same whether fish are present or not. This is the situation that must be treated accurately, and so we assumed that shot noise could be approximated by an additive signal-independent Gaussian process for the purposes of our study. The final noise source is caused by variations of the optical properties of the water with depth. Variations that are slow in comparison with the depth resolution of the lidar can be estimated and eliminated. However, more rapid fluctua-

tions would be indistinguishable from noise. In the absence of a better model for these fluctuations, we also assumed that they were Gaussian. Thus, an additive signal-independent Gaussian noise was considered, and the source of this noise was not considered further. The final results would not be very different if the dominant noise was not Gaussian. Non-Gaussian noise would change the numerical values of the detection and false-alarm integrals. Because of the strong exponential decrease in signal level with depth, small changes in these values would correspond to small changes in detection depth. A similar effect was caused by our choice of threshold level, which also changed the detection and false-alarm integrals. We show that the results are not very sensitive to our choice of threshold level for the same reason. It is possible that the variations in optical properties produce a highly non-Gaussian noise that will have a significant effect, but we have no evidence for this.

The probability density function (pdf) of the instantaneous signal (s) for a single pulse at some depth can therefore be approximated by a normal pdf with mean = S and variance = σ^2 . For illustration, we assumed that σ was not depth dependent, although s clearly was.

Detection was accomplished by setting a threshold signal level above which we asserted that fish were present. The detection probability is the probability that the instantaneous signal is above this threshold when fish are present (i.e. when $\beta_f > 0$). Thus,

$$p(\text{detection}) = P(s > T) = 1 - \Phi\left(\frac{T - S_f}{\sigma}\right),$$

where T = the threshold level;
 S = a normal random variable with mean = S_f and variance = σ^2 ;
 S_f = the signal level with fish present; and
 $\Phi(u) = P(U < u)$ is normal distribution function of U with mean = 0 and variance = 1.

Specifying that fish are present whenever the received signal exceeds some threshold value entails some probability of a "false alarm." This probability can be calculated from

$$P(\text{false alarm}) = P(s > T) = 1 - \Phi\left(\frac{T - S_w}{\sigma}\right),$$

where S_w = the signal from clear water.

To reduce the number of free parameters, we normalized everything by the noise level. Thus, we defined a signal-to-noise ratio, $SNR = (S_f - S_w)/\sigma$

and a threshold-to-noise ratio, $TNR = (T - S_w)/\sigma$. Then $P(\text{detection}) = 1 - \Phi(TNR - SNR)$ for signals following normal distribution with mean SNR and variance 1 when fish are present, and $P(\text{false alarm}) = 1 - \Phi(TNR)$ for signals following normal distribution with mean = 0 and variance = 1 when no fish are present.

The maximum detection depth, z_{max} , was defined as the depth at which the detection probability is 0.5, i.e. the SNR_z is equal to the TNR because of the sharp drop in detection probability from 1 to 0 with depth (Fig. 2).

$$TNR = SNR_z = SNR_0 e^{-2\alpha z}. \quad (5)$$

We could rearrange the terms in Equation 5 and calculate that

$$z_{max} \approx -\frac{1}{2\alpha} \ln\left(\frac{TNR}{SNR_0}\right). \quad (6)$$

We investigated the degree that maximum detection depth for schools is affected by the setting of the false-alarm rate by calculating z_{max} as a function of the false-alarm probabilities and determining the value of TNR to be used in Equation 6. The detection probability ($P(\text{detection})$) can be approximated by unity for depths above this z_{max} and by zero for depths below it (Fig. 2). That is

$$P(\text{detection}) = 1 \text{ for } SNR_z > TNR \text{ or } z < z_{max} \\ = 0 \text{ otherwise.}$$

Laser power and penetration depth

To get an idea of the ranges of depths that might be available to the lidar for a reasonable cost, we calculated the maximum penetration depth (z_{max}) with a lidar model that was developed to perform engineering trade-offs quickly and easily. Input parameters and lidar components can be changed easily by the user, and the computer program automatically calculates all of the affected program quantities. Plots can be quickly generated within the program to allow the results to be immediately viewed. The lidar system was assumed to be similar to that currently used by NOAA (Churnside et al., 1997). Actual parameters are presented in Table 3.

Only laser power effects were considered. Clearly, other factors were also important. These included receiver telescope diameter, detector sensitivity, background light conditions, fish species, density, etc.

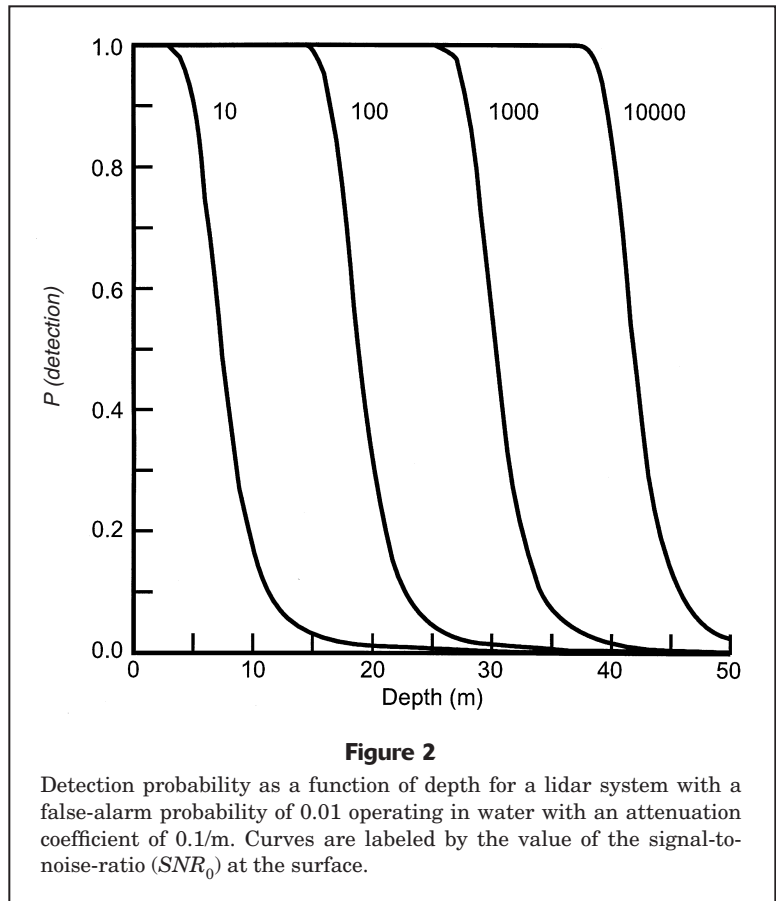


Figure 2

Detection probability as a function of depth for a lidar system with a false-alarm probability of 0.01 operating in water with an attenuation coefficient of 0.1/m. Curves are labeled by the value of the signal-to-noise-ratio (SNR_0) at the surface.

However, a full investigation of the effects of all pertinent parameters was beyond the scope of our study. The effects of some of these parameters, however, could be estimated. Doubling the receiver telescope area, detector sensitivity, or fish density, for example, is equivalent to doubling the laser power, and we could have considered an equivalent laser energy that included differences in these parameters. Because of the assumptions used in our calculations, our calculations should be taken as representative and are not necessarily precise.

Because of the interference with the surface, it was difficult to actually calculate SNR_0 . Instead, we noted that

$$SNR_0 = SNR_z \exp(2\alpha z), \quad (7)$$

where z = any arbitrary depth; and

SNR_z = the signal-to-noise ratio at that depth.

The calculations were done with a fish school deep enough so that surface effects (e.g. specular reflections of the tail of the laser pulse) did not contribute to the received signal from the school. Equation 7 does not hold for fish within about 1 m of the surface,

but the errors are negligible for the depth distributions of fish used in our study.

The signal and noise levels can be defined at any one of a number of points in the receiver, including optical power on the detector, current out of the detector, the voltage generated by that current through a standard 50- Ω resistance, the output of the log-amplifier, or the integer value that this produces when digitized. We consistently used the voltage across 50 Ω , which is the input voltage to the log-amplifier. For an infinitesimally short laser pulse, this signal varies in time as the pulse propagates through the water. We could relate this time to the depth at which the light was scattered back to the receiver because we knew the speed at which light travels through water. Therefore, we could write the signal as a function of depth as for a nadir-pointing:

$$S'(z) = \frac{P(z)\pi d^2 R \beta(\pi)}{4(z + nh)^2} \exp(-2\alpha z), \quad (8)$$

Table 3

Baseline model parameters for computing laser power and penetration depth.

Parameter	Value
Transmitter	
Wavelength	532 nmi
Pulse length	15 nsec
Pulse energy	1 mJ–1 kJ
Pulse repetition rate	10 Hz
Height above surface	100 m
Beam divergence	25 mrad
Receiver	
Aperture diameter	20 cm
Field of view	25 mrad
Optical bandwidth	10 nm
Electronic bandwidth	100 MHz
Sample rate	1 GHz
Receiver noise	140 microvolts
Detector type	R5800 photomultiplier tube @ 1200 V
Polarization	Unpolarized
Environment	
Aircraft height	100 m
Water type	IB, III
Background light	1/4 moon
Background light fluctuations	2 percent
Fish school	
Fish type	anchovy
Length	10 cm
Reflectivity	
Packing density	0.5/ m ³
School thickness	10 m

where S' = the received signal per unit depth at depth z ;

P = the laser power;

R = the responsivity of the detector and load in V/W;

$\beta(\pi)$ = the backscatter coefficient of the water plus any fish present at that depth;

h = the height of the aircraft above the surface;

n = the index of refraction of water (1.33); and

α = the lidar attenuation coefficient.

To get the actual signal voltage, we had to integrate Equation 8 over the finite duration of the laser pulse. To get the short pulses desired, it was necessary to use Q-switching. With this technique, the laser resonator is blocked electro-optically while the energy is stored in the lasing medium. The cavity is then quickly opened. Lasing begins rapidly, and the output power quickly builds to a high value. As the energy in the lasing medium is depleted, the output power decreases back to zero. This technique produces a characteristic pulse shape that can be approximated by

$$P(t) = \frac{Et}{\tau^2} \exp\left(-\frac{t}{\tau}\right), \quad (9)$$

where E = the total pulse energy; and

τ = 0.408 times the full width of the pulse at one half of its maximum value.

We converted this time to distance through the speed of light, and integrated Equation 8 over depth.

Two water types were used. These were Jerlov (1968) types IB and III. These specify only the diffuse attenuation coefficient K_D . To obtain an estimate of lidar attenuation we needed to have an estimate of the volume scattering function $\beta(\vartheta)$, where ϑ is the scattering angle. We used the general functional form of Petzhold (Petzhold, 1972; Mobley, 1995) with the exact values scaled by the value of the scattering coefficient inferred from the different values for K_D . We first noted that

$$K_D = a + 2\pi b \int_{\frac{\pi}{2}}^{\pi} \frac{\beta(\theta)}{b} \sin(\theta) d\theta, \quad (10)$$

where a = the absorption coefficient of sea water;

b = the scattering coefficient; and

$\beta(\vartheta)/b$ = the normalized scattering function of Petzhold.

From this expression, we obtained the scattering coefficient and the backscatter coefficient for each of the Jerlov water types. The beam attenuation coefficient is given by

$$C = a + b. \quad (11)$$

The lidar attenuation coefficient lies somewhere between the diffuse attenuation coefficient and the beam attenuation coefficient in such a way that it depends on the beam divergence of the lidar and on the spot size of the laser at the surface. The details of this dependence are not completely understood, and therefore we made what we hoped were reasonable estimates. Following Feigels and Kopilevich (1994), we estimated the divergence angle effect for a beam of negligible size by assuming that photons scattered at angles greater than the lidar divergence angle $\Phi/2$ are lost. We then applied a correction to this value for the finite size of the spot at the surface based on a curve fitted to the results of Gordon (1982). The final result was an estimate for the lidar attenuation coefficient given by

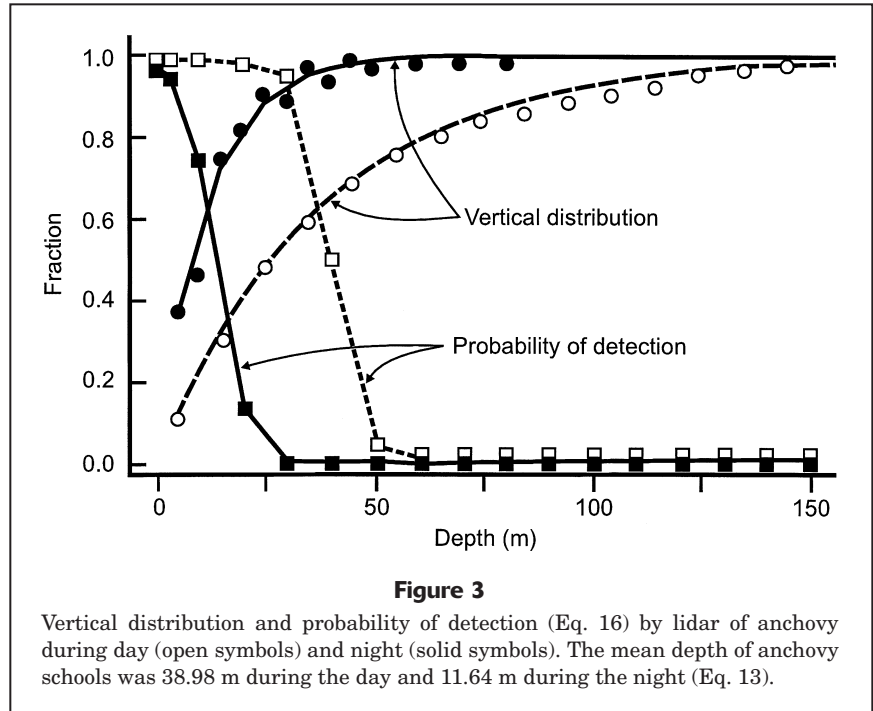
$$\alpha = K_D + 2\pi b \exp(-0.8c\phi h) \int_{\frac{\phi}{2}}^{\frac{\pi}{2}} \frac{\beta(\theta)}{b} \sin(\theta) d\theta, \quad (12)$$

where h = the height of the lidar above the surface.

The results were fairly sensitive to this parameter; a factor of 2 in α is equivalent to a factor of 2 in depth penetration. The values used in our study were consistent with observations in the Southern California Bight, and are representative of what can be expected. However, more work is needed before accurate predictions of detection probability can be made for a specific water mass based on measurements of the optical properties. Direct measurements of α can provide better detection predictions and can also be used to refine this relationship.

Vertical distribution and packing density of fish schools

The vertical distributions of schools below the surface, their packing density, and fish size are critical biological properties affecting detection of schools



with a lidar. Two vertical distributions of anchovy fish schools were used in our analyses. One represented an average distribution of anchovy schools during the day and the other, average distribution of anchovy schools during the night (Fig. 3). The daytime vertical distribution fitted the average of the cumulative proportion of fish schools during the May 1997 and September 1997 surveys of Holliday and Larson (1979), who used the acoustic reflection from the bottom as a better way to probe the upper 10–20 m than that afforded by conventional acoustic methods. The nighttime vertical distribution curve fitted the cumulative proportions of newly spawned anchovy eggs from two California sites (Pommeranz and Moser, 1987) and anchovy schools from three anchoveta acoustic surveys in Peru (Castillo Valderama, 1995). The depth of early-stage anchovy eggs may indicate school depth because anchovy spawn during the night. Vertical distributions during the daytime and nighttime were fitted to an exponential distribution function:

$$F(z) = p(Z < z) = 1 - \exp(-z/\lambda), \quad (13)$$

where $F(z)$ = the proportion of fish schools in the upper z meter depth; and λ = the mean depth of the fish schools.

Direct measurements of school packing density (numbers of fish/m³) for anchovy were taken from the literature (Table 4). Graves (1977) deployed a

Table 4

Estimated mean, standard deviation (SD) of packing density(x ; fish/m³) of anchovy and herring, and the log-transformed data ($y=\ln(x)$) during day and night. Coefficient of variation (CV)= SD/mean.

Species	Night or day	Packing density(x)			$y=\ln(x)$		Fish length (cm)	Reference
		mean	SD	CV	mean	SD ¹		
Anchovy	night	53	0.257 <i>n</i> =5	0.48	-0.74	(0.52) 1.11	10	Aoki and Inagaki, 1988
Anchovy	day	114.8	99 <i>n</i> =10	0.86	4.505	(0.67) 1.11	10	Graves, 1977
Herring	day	2.57	3.99 <i>n</i> =20	1.55	0.0725	1.344	3	Misund, 1993

¹ 1.11=sqrt(ln(1.55² + 1)), where 1.55 is the CV for 34-cm herring (Eq. 14). Values in parentheses were computed from original data sets.

“dropped” camera by day and Aoki and Inagaki (1988) used a tethered camera by night and obtained the packing density of anchovy with an average length of 10 cm.

The standard deviations (SD) of packing density of anchovy computed from data collected by Aoki and Inagaki (1988) and Graves (1977) measured only the variation among schools and would underestimate the overall variation of packing density. For this reason, we used the coefficient of variation of packing density of herring (1.55) (Misund, 1993; Lo et al.²), a more realistic measurement of the variation of packing density, together with the mean packing density of anchovy to estimate the mean (μ_y) and variance (σ_y^2) of log-transformed data: $y = \ln(x)$, where x is the packing density for 10-cm anchovy:

$$\hat{\sigma}_y^2 = \ln[CV^2(x) + 1], \tag{14}$$

$$\begin{aligned} \hat{\mu}_y &= \ln(\bar{x}) - \hat{\sigma}_y^2/2 \\ &= \ln(\bar{x}) - \ln(CV^2(x) + 1)/2, \end{aligned} \tag{15}$$

where $CV(x)$ was that of herring (=1.55). Equations 14 and 15 were derived from the following two relations:

$$\begin{aligned} \mu_x &= \exp(\mu_y + \sigma_y^2/2) \text{ and} \\ \sigma_x^2 &= \exp(2\mu_y + \sigma_y^2)[\exp(\sigma_y^2) - 1]. \end{aligned}$$

Depth-specific probability of detection ($p_a(z)$) based on packing density

As mentioned in an earlier section, $P(\text{detection}) = 1$ for $SNRz > TNR$, and zero otherwise, because the steep drop of $P(\text{detection})$ around z_{max} , the proportion of fish

that can be detected and identified at depth z , $p_a(z)$, was modeled by the $P(SNR_z > TNR)$. The probability of detection ($p_a(z)$) was computed by means of the probability density function of fish packing density (x) at depth z , assuming that SNR_0 is proportional to the packing density (x), i.e. $SNR_0 = Ax$, where A is the proportionality and is a function of fish size and reflectivity. If reflectivity is the same for all fishes, then A is a function of fish size only, $A \sim 10^4 \times L^2$, where L is the fish length in meters (Churnside et al., 1997). The packing density, x , is a lognormal random variable. We could write $SNR_z = SNR_0 \exp(-2z\alpha) = Ax \exp(-2z\alpha)$; thus $SNR_z > TNR$ is equivalent to $x > (TNR/A)\exp(2z\alpha)$, and we approximated the proportion of fish detected at depth z on the basis of the lognormal distribution of packing density (x) by

$$\begin{aligned} p_a(z) &= \int_{\exp(2\alpha z)TNR/A}^{\infty} p(x)dx \\ &= P(\ln(x) > [2\alpha z + \ln(TNR / A)]) \\ &= 1 - \Phi\left(\frac{2\alpha z + \ln(TNR / A) - \mu}{\sigma}\right), \end{aligned} \tag{16}$$

where $\Phi(u) = P(U < u)$ for the normal random variable, U , with mean = 0 and variance = 1; and

$\ln(x)$ has mean μ and variance σ^2 .

Equation 16 was computed through SNR_z , the mean of each individual normalized signal (or pulse). In the appendix of this paper, we computed $P_a(z)$ through individual normalized signals. We also assumed with this computation that the effects of shadowing could be neglected. Although more work on this issue is needed, our results suggest that it is not a serious effect. We observed multiple layers of fish in our

data, suggesting that light was penetrating the first layer. We also observed that the water returned from below and above schools of fish and found that the additional attenuation caused by the fish was small in comparison with the background water attenuation.

Proportion of fish schools detected (q)

The proportion of fish schools detected in the upper z meters (q_z) depends on the depth-specific probability of detection ($P_a(z)$; Eq. 16) and the vertical distribution of fish schools (Eq. 13).

The quantity (q_z) was computed by numerical integration:

$$q_z = \int_0^z P_a(u) f(u) du \quad (17)$$

$$= \int_0^z \left[1 - \Phi \left(\frac{2\alpha u + \ln(TNR/A) - \mu}{\sigma} \right) \right] \frac{1}{\lambda} e^{-\frac{u}{\lambda}} du,$$

where $p_a(u)$ is derived from Equation 16 and $f(u)$ is the exponential pdf derived from Equation 13:

$$f(u) = \frac{1}{\lambda} e^{-\frac{u}{\lambda}}. \quad (18)$$

The quantity, q_z , increases with depth z and reaches an asymptote at z_{max} ($q; q \leq 1$) and q is defined as the proportion of fish schools detected.

Criterion for evaluating trade-offs between penetration depth and swath width

If laser power is held constant, an increase in swath width would decrease the maximum depth of penetration of the laser pulse. In this section, we established a criterion for comparing various instruments having different combinations of swath width and laser power (maximum penetration depth). The effectiveness of the width of a swath (y) can be measured by the probability that some fish schools will be encountered (p_y) in the swath (Eq. 1 from simulation). The effectiveness of a lidar in detecting schools within the swath is measured by the proportion of fish schools detected (q) (Eq. 17). The product of p_y , q (Eqs. 1 and 17) is then used to evaluate the overall effectiveness of any instruments with a given swath width (y).

Results

Effects of swath width on encounter probability

We assumed that schools were aggregated into school groups in the survey area (42,204 km²) and that

school diameters and densities were equal to, or less than, those reported by Smith (1981). Our simulation results indicated that swath width had little effect on the probability of encountering schools. This was true for all three population sizes: 16,000, 32,000, and 80,000 schools (Fig. 4). Encounter probability was affected by the swath width only when the diameters of the school groups were small and the school density within the school group was so low (both multipliers were 0.5) that their distribution became nearly random rather than aggregated. In these cases, the encounter probability increased sharply when the swath width increased from 1 m to 50 m. Even this very limited effect of swath width diminished as the number of schools in the survey area increased. The encounter probability for swath widths greater than 50 m was almost constant regardless of conditions.

For the multiple swaths, the probability that at least one of them would intercept anchovy schools (Eq. 2) was high in general. The lowest probability was 0.65, for the case where fish were aggregated in few large school groups of low population, i.e. 16,000 (1.5,1.5) for $n=5$ (Eq. 2). For $n=10$, the probability ($p_{y,n}$) was close to one for all cases.

Depth-specific detection probability

The depth at which a lidar is capable of detecting a school or target will depend in part on the threshold setting of the instrument in relation to the noise (TNR). To illustrate these relationships we fixed a false-alarm rate ($P(\text{false alarm})$) for the detection of schools, used an alarm rate to determine the threshold level, and then calculated the detection probability for schools ($P(\text{detection})$). The results of such a calculation are presented in Figure 5, where the detection probability for fish schools was plotted as a function of the probability of a false alarm for signal-to-noise ratios of 1 and 3. Zero, the lower limit of the plot, corresponds to a very high threshold (TNR) setting, where the probability of a false alarm and the probability of detecting a school are both zero. We concluded that fish are never present at a setting of zero. The upper limit of Figure 5 corresponds to a very low threshold setting, where $P(\text{false alarm})$ and $P(\text{detection})$ are both unity; at a setting of 1, we concluded that fish are always present.

If one selects a reasonable false-alarm rate and a signal-to-noise ratio at the surface, one can calculate the detection probability as a function of depth. This was done for a false-alarm probability of 1% and a lidar attenuation coefficient of 0.1/m, and the results are plotted in Figure 2 for several values of the surface signal-to-noise ratio. There are several interest-

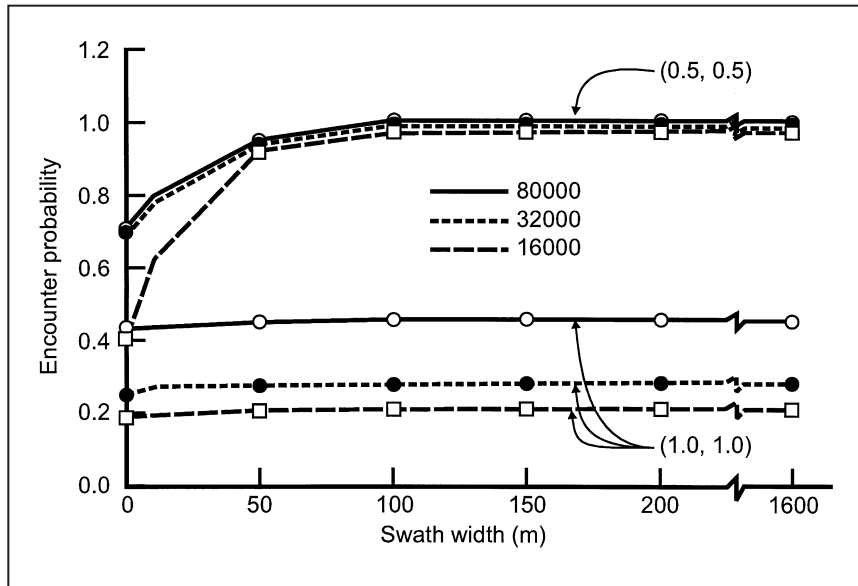


Figure 4

Simulated encounter probability of anchovy schools in Los Angeles Bight (Table 2) for 16,000, 32,000, and 80,000 schools. The swath width ranged from 1 m to 1600 m. The multiplier for mean and standard deviation of the log of diameter of school group and the log of school density in a school group are given in parentheses. Values for populations with multiplier (1.5,1.5), similar to populations with multiplier (1.0,1.0), are not shown.

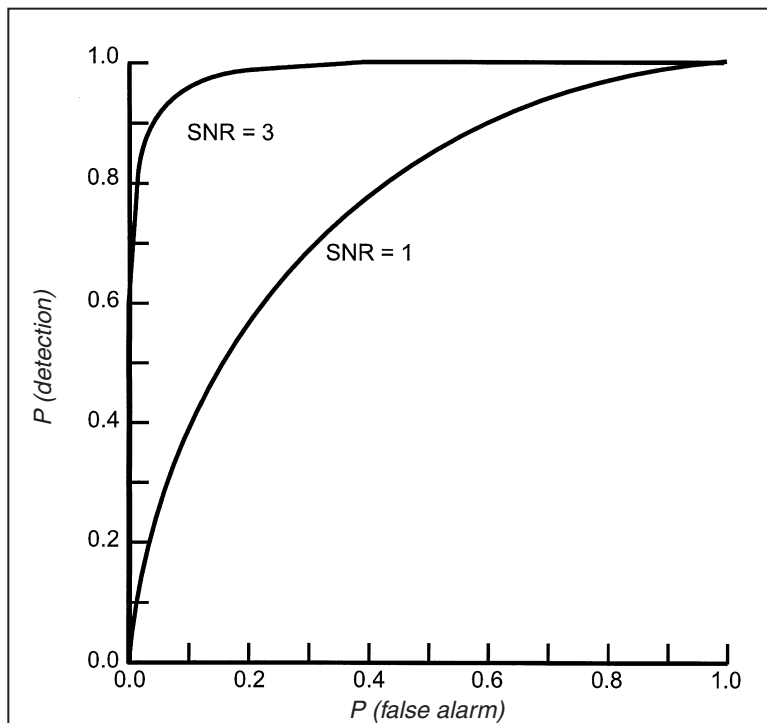


Figure 5

Detection probability as a function of the false-alarm probability for lidar systems with signal-to-noise-ratios (SNR) of 1 and 3.

ing features of these results. The first is that when a critical depth is reached, the detection probability drops abruptly from nearly unity to nearly zero over a narrow, 5–10 m span of depth. Because of this sharp transition, we defined a maximum detection depth (z_{max}) as the depth at which the detection probability is 0.5. The depth z_{max} depends logarithmically on signal level because of the exponential attenuation of the signal with depth. Thus, each order-of-magnitude increase in signal level (illustrated in Fig. 2) provides an increase in z_{max} of just over 10 m in depth. Ten meters is just about 1 lidar attenuation depth, defined as $1/\alpha$ (Eq. 6). We can rewrite Equation 6 as $z_{max} = \ln(SNR_0/TNR) \times 0.5/\alpha$. Therefore, if the attenuation coefficient (α) is different from 0.1/m, the value used in our study, these z_{max} depth values scale linearly with lidar attenuation depth ($1/\alpha$).

To examine the sensitivity of z_{max} (Eq. 6) to TNR and thus the false alarm probability (Eq. 6), we used the same values of the surface signal-to-noise ratio as those used in Figure 2. This calculation indicated that the maximum detection depth (z_{max}) was relatively insensitive to changes in false-alarm probabilities. Decreasing the false alarm rate by a factor 10 from 0.01 to 0.001 would only increase the maximum detection depth by a few meters (Fig. 6). Thus, a fairly low rate of false alarms for a system could be selected without seriously degrading the detection performance. It also implied that we could select a nominal threshold level and obtain a simple expression for the maximum detection depth. A value of $TNR = 3$ results in a false-alarm probability of just above 0.1%. Therefore, according to Equation 6, z_{max} is determined by

$$z_{max} \approx -\frac{1}{2\alpha} \ln\left(\frac{3}{SNR_0}\right). \quad (19)$$

We then considered the depth in the water column at which schools can be detected by

a single lidar pulse and computed, using Equation 16, the proportion of fish schools that could be detected for anchovy (Fig. 3). During the daytime, and at a depth of 30 m, 97% of 10-cm anchovy would be detected ($p_a(z)$, when $\alpha=0.1/\text{m}$). Moreover, one can also compute a signal-to-noise ratio from the packing density(x): $SNR_z = Ax \exp(-2\alpha z)$ for a fish length of 10 cm and compare it to the threshold target-to-noise ratio (TNR) of 3. At the surface, SNR_0 was 11,480 for 10-cm anchovy and $z_{max} = 41.24$ m. At a depth of 30 m, SNR_{30} ($\alpha=0.1$) was 28.5, which was above $TNR = 3$, indicating that most of the schools in the upper 30 m could be detected. The detection probability for anchovy was unity over the upper 30 m (Fig. 3), which was consistent with the results we obtained from Equation 16 (Fig. 3).

For the schools at night, we used a very low packing density (0.53 anchovy/ m^3). The signal-to-noise ratio at the surface (SNR_0) for such diffuse schools was 53, substantially above a TNR of 3, and $z_{max} = 14$ m. At 20 m, the SNR_{20} for anchovy schools declined to 0.97 with a probability of detection of only 13%. At 30 m, the detectability of anchovy was less than 1%.

Overall vulnerability of schools to lidar detection in the vertical plane

We estimated the cumulated proportion of schools of anchovy that might be detected by a lidar assuming constant day and night vertical distributions. As the first step in the discussion that follows, we focused on the two components used to make the estimate: 1) the average vertical distributions of schools of anchovy during the day and the night (Fig. 3; Eq. 13); and 2) the depth-specific probability of detecting a school, which was discussed in the previous section (Eq. 16). These two components were combined to obtain the final estimates.

The probability of detecting a school during the day declined from about 1 at the surface to 0.50 at 40 m and approached zero at 60 m ($\alpha=0.1$, Eq. 16; Fig. 3). Because of the lower packing density of the school, the depth-specific probability of detecting a school was much lower at night (with the detection probability dropping from 1 at the surface to 0.10 at 20 m and zero at 30 m). Thus, even the very diffuse nighttime aggregations of anchovy (0.53 fish/ m^3) observed by Aoki and Inagaki (1988) could be distinguished from background noise. That shallow night-

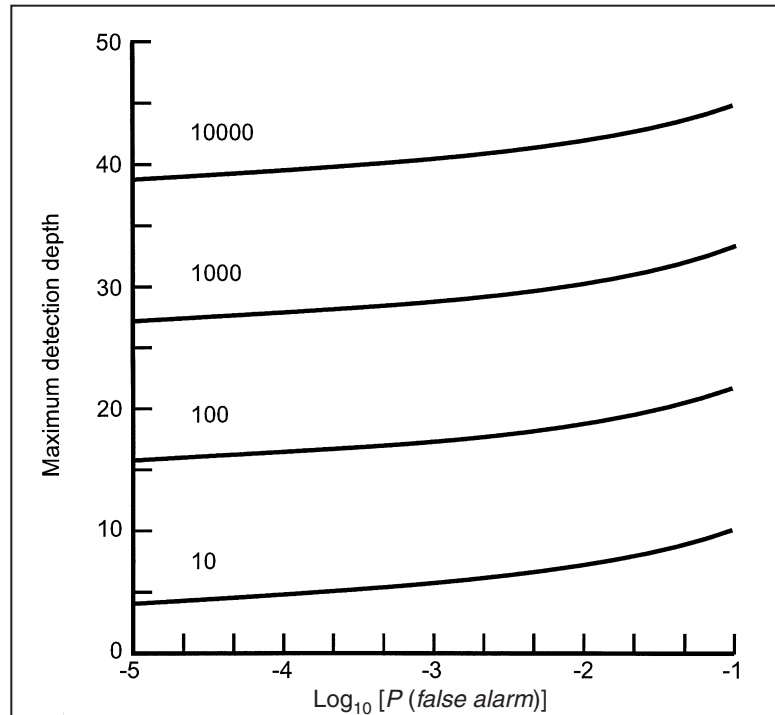


Figure 6

Maximum detection depth as a function of the false-alarm probability for a lidar system operating in water with an attenuation coefficient of 0.1/m. Curves are labeled by the value of the signal-to-noise ratio (SNR_0) at the surface.

time schools can readily be detected by an airborne lidar despite their low packing density means that during the night lidar surveys are feasible.

By combining the detection probabilities with the vertical distributions (Eq. 17), we could calculate the proportion of anchovy schools that could be detected (q) by the lidar (Fig. 7). This calculation indicated that a lidar survey at night would be more accurate than one during the day because the cumulated proportion of schools detected during the night was 60% in the upper 20 m, whereas during the day, it was 40% in the upper 20 m. Thus, despite the higher packing density in the day (115 fish/ m^3) which permitted detection down to about 50 m, schools were detected more often at night. This feature was due to the difference in vertical distributions between night and day.

Up to this point we have discussed only cases in which the lidar attenuation coefficient, α , equals 0.1/m, a typical value for the coastal waters of southern California. To illustrate the effect of water clarity, we varied α from 0.05 to 0.6, where the attenuation coefficient for the most turbid coastal water was 0.52. Generally, the proportion of anchovy schools detected (q) declines rapidly with increasing α , although detection also depends on the design

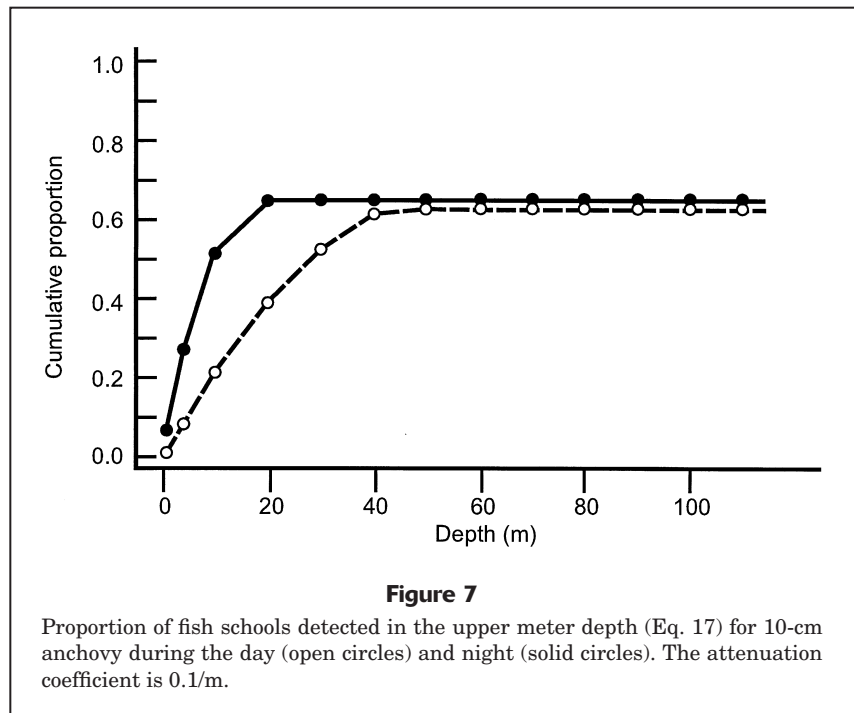
and settings of the lidar as well. Some generalizations can be made. During the night the lidar field of view can be large because less background light exists to interfere with the signal. Under these conditions, the lidar attenuation coefficient (α) will be very nearly equal to the diffuse attenuation coefficient. For the Jerlov open-ocean water types at 532 nmi, α varies from about 0.05/m (type I) to about 0.11/m (type III). The values for the Jerlov coastal water types range from 0.15 (type 1) to about 0.53 (type 9). From our analysis, we expected that most anchovy schools would be detected during the night in the open ocean for $\alpha \leq 0.1$.

During the day, the situation is more complicated. A lidar system with a large field of view will have a smaller signal-to-noise ratio because scattered sunlight reaches the receiver. We could have increased the signal to noise by decreasing the field of view, but this would tend to increase α . Besides, an increase in the signal-to-noise ratio during the day would have little effect on q , because the vertical distribution of schools during the day has a long tail extending down to 155 m (Castillo Valderrama, 1995). At night, an increase in the signal strength that extends the maximum depth of a return by 10 m or so could have an important consequence because of shallow vertical distribution (82% of the school are in the upper 20 m).

Comparisons with vision-based methods

We compared the ability of a human observer to count fish schools with the capability of a lidar. Hara (1990) reported that an observer flying at 500 m would be able to detect sardine schools along a 1600-m swath and to a depth of about 4 m. We assumed that all schools at 4 m could be detected visually and none was detected below that depth. For the lidar, we used a swath width of 7 m, and we considered the product of encounter probability (p_y) (Eq. 1) depicted by swath width and the maximum proportion of schools detected (q) depicted by depth (Eq. 17) to be a measure of the overall performance.

A human observer detects somewhat more schools in the horizontal plane than does a lidar system because of the relatively large swath width provided by aerial viewing (Table 5). The encounter probabilities in the horizontal plane (Eq. 1) obtained from



simulation for a population of 32,000 schools was 0.51 for visual detection and 0.42 for lidar detection. In the vertical plane, however, our analysis demonstrated that lidar is superior in detecting schools both during the day and night. During the night, the proportion of anchovy schools detected (q) by the lidar was 0.65, whereas it was 0.28 for the human observer. The difference between visual detection and lidar detection was much greater during the day (q was 0.63 for the lidar), whereas that for the observer was only 0.095.

The $p_y q$ (an overall measure of detection performance) for a lidar was at least 1.9 times that of an aerial observer. This means on the average that the proportion of anchovy schools detected during a survey would be about twice as great for a lidar as it would be for an aerial observer.

We have considered here, however, only one aspect of the two systems—detection rates. Many other differences also exist in relation to species identifications, biomass, and effects of environmental conditions on the observing system.

Laser power and penetration depth

A set of parameters used to compute the laser power and penetration depth for schools of anchovy is listed in Table 3. The lidar signal was computed by using Equation 8, and the penetration depth was computed from the attenuation coefficient estimated from Equation 12. The relation of penetration

Table 5

Comparison of the effectiveness of lidar and aerial observation with different swath width (y) and depth penetration for 10-cm anchovy during the night and day. p_y is the probability of encountering schools for a population of 32,000 schools and swath width y . q proportion of fish school detected for $\alpha = 0.1$ and 0.05 , where α is the instantaneous attenuation rate per meter. The product, $p_y q$, is used to evaluate the efficiency of instruments.

Lidar aerial ratio	Maximum detection depth (m)	Swath width (y) (m)	p_y	Proportion of fish schools detected (q)		Overall efficiency ($p_y q$)	
				night	day	night	day
$\alpha=0.1$							
Lidar		7	0.42	0.65	0.63	0.27	0.26
Aerial	4	1600	0.51	0.28	0.095	0.14	0.048
Ratio						1.92	5.410
$\alpha=0.05$							
Lidar		7	0.42	0.84	0.85	0.35	0.35
Aerial	4	1600	0.51	0.28	0.095	0.14	0.048
Ratio						2.44	7.50

depth and the logarithmic laser energy for both open ocean and coastal waters was obtained (Fig. 8). Calculations of SNR_0 were made at two laser power levels, and logarithmic dependence was used to generate the curves.

We calculated the maximum penetration depth for the NOAA lidar with a power of 67 mJ and scaled that depth with laser power (Churnside and Hunter, 1996; Table 3). For this calculation, we assumed the presence of 10-cm anchovy with a packing density of $0.5/m^3$ (Table 3). Night flights at 100 m altitude were also assumed. Two water types were used, one typical of open ocean water (Jerlov type IB) and one more typical of coastal water (Jerlov type III) (Jerlov, 1968).

The NOAA lidar presently in use is capable of operating from a single-engine plane; it weighs about 100 kg, requires less than 1 kW of power, and the cost of its components is about \$50K. The penetration depth for this system under these somewhat optimum conditions is estimated to be about 45 m at 67 mJ (Fig. 8). Some cost can be saved by using a lower-power laser and smaller telescope, but not a great deal.

A savings of only about \$10K is likely even if one uses an equivalent energy of 1 mJ. This amount of energy still provides close to 32 m of depth penetration for the conditions assumed in our study.

On the other end, one can obtain approximately 57 m of penetration by using a system with an equivalent pulse energy of 100 J (Fig. 8), but such a system would be a very large and expensive to set up

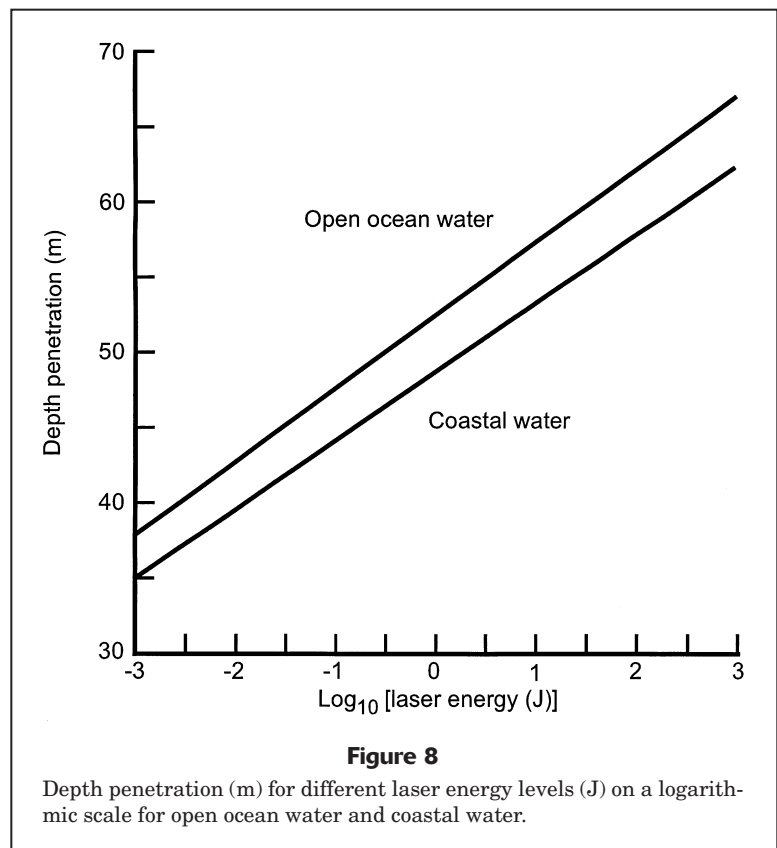


Figure 8
Depth penetration (m) for different laser energy levels (J) on a logarithmic scale for open ocean water and coastal water.

and operate. Part of the equivalent energy could be obtained by using a larger telescope at a power only a little over an order of magnitude of that currently used—one that would emit a laser energy of 10J. This type of laser would require a custom design, with a cost that we estimated to be in the order of one million dollars. In addition, it would require about 100 kW of power, which cannot be supplied by a small,

single-engine aircraft. An aircraft something like the DeHaviland Twin Otter may be necessary to accommodate the size and power requirements of the NOAA lidar system. The system size and cost would probably increase significantly at an equivalent energy of about 1 J. Thus, a practical range for penetration depths would be between about 35 and 50 m.

Discussion

Interpretation of modeling results

Our goal was to model various aspects of a lidar survey system for anchovy with a focus on features that might affect survey accuracy and precision. We learned from our modeling of swath width that this width has little or no effect on the rate at which schools are encountered when they are aggregated into school groups, as is commonly the case with small pelagic fish, like sardines and anchovy, except under very low biomass levels. Under conditions of very low biomass, schools may become scattered rather than aggregated, in which case encounter rates would increase with swath width. Our analyses also showed that the chance that all the transects would not intercept any fish school was extremely small because the number of transect lines is likely to be much greater than 5, owing to the high speed of the survey airplane. Thus, from the standpoint of survey precision, swath width may be given a low priority.

Lack of full vulnerability to the counting technique is one of the most important potential sources of bias for biomass surveys. Fish may not be fully vulnerable because the survey does not extend over the full geographic range of the stock and because there are limitations to the counting system. Nearly all fishery-independent surveys suffer to some extent from these problems. In the case of an airborne lidar survey, the depth limits of the sensing system could produce a large potential bias, particularly if the system is used during the day. Our model indicated that, on average, 36% of schools of anchovy during the day would be expected to be below the maximum detection depth of the lidar ($z_{max}=41$ m) (Figs. 3 and 8). Because the vertical distribution of schools can vary considerably between surveys, the undetected fraction would vary, thus affecting survey accuracy. This computation is driven by our vertical distribution curve for the daytime and the rapid attenuation of light in water; packing density and fish size have negligible effects. Thus, a reliable estimation of the biomass of such small schooling fishes during the day in offshore waters does not seem practical unless a reliable unbiased estimate of vertical distribution of schools

is available. On the other hand, in water up to 30 m depth over the shelf, accurate estimates of biomass for the daytime are practical because the vertical movements of the fish would be restricted.

If a lidar survey were restricted to night flights, when schools are closer to the surface, the bias caused by the uncounted fraction of deep schools would be considerably reduced. During the night, however, schools may become very diffuse and consequently have a much lower target strength which reduces their detectability. The good news from our modeling work was that even the very diffuse schools of 10-cm Japanese anchovy ($0.53/\text{m}^3$, Aoki and Inagaki, 1988) at night were detectable over the upper 20 m. Our model indicated that 65% of all anchovy schools would be detected during the night.

In our study, we focused only on 10-cm anchovy schools at two known and widely differing packing densities and vertical distributions. We ran our models with other packing densities and fish sizes, using data from herring, sardine, and mackerel but keeping the vertical distributions the same as that for anchovy.² These results indicated that packing density is an important factor in the detection of schools at night when the vertical distribution is shallow but is unimportant during the day when fish have a deeper vertical distribution. The effect of packing density at night can be significant. For example, at night at 30 m the SNR for schools of 10-cm anchovy (packing density 0.53) was only 0.97, whereas that for 13-cm sardine (4.0 packing density) was 12.38 (their detectability was 13% and 77%, respectively). Schools of small fishes may be inherently more detectable than those of larger fish because the decline in average packing densities of schools with increasing fish size is not completely compensated by the increase in reflective area of the fish (packing density changes in proportion to $1/L^3$ (Misund, 1993), whereas the reflective area changes in proportion to L^2). However, this theoretical relationship is eclipsed by the huge variation in packing density due to behavioral factors. The density of anchovy schools at night varies from compact schools suitable for capture by the purse-seine fishery (Squire, 1972) to schools so diffuse that many authors have concluded that schooling ceases (Whitney, 1969; Baxter and Hunter, 1982). The packing density used in our example of an anchovy school at night from Aoki and Inagaki (1988) represents such an extremely dispersed state, but dense concentrations of anchovy do occur at night, only their packing density has not been measured. In fact, 4 fish/ m^3 used in the sardine night example might be equally appropriate for anchovy. Unfortunately, because field measurements of packing densities at night are so infrequent, it is impossible to tell at this

point where the mean may fall or what differences might exist between species.

Detection of schools during the night would improve if maximum schooling depth and α were correlated as Hunter and Nicholl (1985) speculated. They determined the visual threshold for schooling in northern anchovy ($6 \times 10^{-11} \text{W/cm}^2$) and suggested that maximum nighttime depth was a function of the ability of fish to see one another. They estimated that the visual threshold for schooling would occur at 38 m during a full moon and at 30 m on a starlit night where chlorophyll was 0.2 mg Chla/m^3 and at 8 m (starlit) and 20 m (full moon) when chlorophyll was 2.0 mg Chla/m^3 . If Hunter and Nicholl (1985) are correct, then the maximum lidar detection depth should increase as the schooling depth increases at night, as long as survey flights are made under the same moon phase. This relationship between visual threshold and moon phase also indicates that it may also be important to exclude survey nights during a full moon—a rule long observed by pilots who locate schools for the fishing industry.

It may be possible in practice to detect schools somewhat deeper than those that our model indicates because the model estimates the detection of a single pulse at one range gate or depth. In practice, a lidar will generate a composite image of a school derived from a number of such pulses over a range of gates (depths) analogous to an echogram trace. Such a composite image produced from multiple returns and gates can be more readily separated from background noise than can a single pulse, but such a separation involves a more complex, and at the present time, somewhat more qualitative discrimination process. Signal-processing algorithms can be developed for this application, but their performance would depend on the exact algorithm used. More accurate estimates of detection depth would depend upon the development of such signal-processing algorithms. Development of such algorithms is one of the most promising directions for future research on fisheries lidar. Their development would greatly improve both the accuracy and precision of future lidar surveys for fisheries, as well as reduce the work in processing images. Similarly, a more thorough understanding of the causes of the observed variation in the vertical distribution of fish could improve survey accuracy and precision. The phase of the moon, time of day, mixed layer depth, temperature, location of forage, fish size, season, and spawning habitats, may all influence where in the water column a school may be found.

It seems unlikely that depth of detection will be greatly improved by increasing sensitivity or power of a lidar system over the basic radiometric system used in our model. Our analysis indicated that an

order of magnitude increase in equivalent laser power (laser power plus sensor changes) would gain about 10 m in detection depth. Such a change would require a custom, rather than an “off-the-shelf” laser, which would cost around a million dollars, in addition to associated costs, including a larger aircraft to satisfy the new power and weight requirements. In addition, increasing the depth of penetration by 10 or 20 m, on the average, would not increase the numbers of schools detected by more than about 10% during the day because school distributions tend to be skewed with a long tail extending to depths far beyond the practical limits of lidar detection in coastal waters. A 10-m gain would be more significant during the night but may not be worth the additional cost.

We have treated the failure of a lidar to count deep schools as a potential bias, which is true unless an unbiased estimate of the mean vertical distribution of schools exists for the particular survey region and season and an appropriate statistical model is used for the survey. When these conditions are met, the failure of a lidar to count deep schools becomes a matter of precision rather than bias. An unbiased estimate of the mean vertical distribution of schools could be estimated from data generated by lidar and acoustic surveys for the same region because by combining the two surveys, one corrects for the vertical bias in each. The appropriate statistical model for a lidar survey would be one based on line transect theory (Buckland et al., 1993). Line transect theory usually deals with encounter rates on the horizontal plane, and animals are assumed to be uniformly distributed in space. In the case of lidar, we turned the model on its side and used an average vertical distribution of anchovy schools in the survey area. An empirically derived vertical distribution does not seem to be subject to any more bias than a uniform, horizontal distribution, one that is commonly assumed in line transect surveys.

To provide indices of relative abundance based on airborne lidar is an important fishery application that is less demanding than that of estimating biomass. For an index of abundance, the extent to which schools are available for counting is not a major concern. Lidar seems uniquely well-suited for taking an inventory of the juveniles of small pelagic fishes (pre-recruits) because they are extremely patchy and tend to inhabit shallow water near the coast in areas difficult to sample with a research vessel. Lidar surveys can provide useful indices of adult biomass as well. Aerial observations (Lo et al., 1992) and passive imaging (Nakashima, 1990; Nakashima and Borstad⁷)

⁷ Nakashima, B. S., and G. A. Borstad. 1993. Detecting and measuring pelagic fish schools using remote sensing techniques. ICES Report C.M. 1993/B:7, session T, Fish Capture Committee, 18 p.

from aircraft are currently used in several fisheries as indices of the abundance of small pelagic fishes and a lidar-based system would have several advantages over these passive methods. Our computation with a deterministic model showed that a lidar survey may be about twice as efficient in detecting schools as a vision-based system during the night and five times more efficient during the day. At night, a lidar will detect more schools than an observer, but the difference is not huge because the very wide swath width (1600 m) of our hypothetical aerial observer compensated, to some degree, for the observer not seeing farther beneath the surface. During the day, the efficiency of lidar detection, in contrast to visual detection, increases greatly because schools inhabit deeper water. In addition to increased detection efficiency, lidar has several other advantages over aerial observers: lidar images can be better quantified than those based on visual detection or cameras because the school volume rather than school area can be estimated, thereby improving the precision of the index; in addition, detection is less dependent on sea state and is little affected by sun angle or moon phases. On the other hand, skilled fishermen working in aerial surveys can identify species of schooling fish with remarkable accuracy; a remote species identification algorithm for a lidar will be difficult, if not impossible, to develop.

As with hydroacoustic methods, species identification with lidar is a major concern. Even after 50 years of hydroacoustic research, the only method for identifying acoustic targets with certainty is by securing voucher specimens. Radiometric backscatter has no magical properties in relation to those of acoustic backscatter that might allow a rapid solution to the problem of species identification. The lesson learned from hydroacoustics is that for species identification to be a reality in lidar surveys, additional sensing systems will be needed. That skillful humans make accurate species identifications visually provides the hope that species recognition algorithms eventually will be practical. We believe it will be possible over the long term to develop species recognition algorithms for lidar in combination with advanced lidar signal processing, digital video cameras, and local knowledge, but at present species identifications must depend upon combining lidar survey data with other information. From the lidar data, we could distinguish reliably between small (about 30 cm length) and large (about 1-m) fish. Identification of intermediate lengths may become possible with more practical experience. One possible approach for obtaining additional information is to use visual identifications of fish schools by aerial observers projected to lidar targets. Other possible approaches are to combine airborne lidar survey with a research trawler

that can provide voucher specimens or to combine airborne lidar with simultaneous sampling of fish eggs from a research vessel (Checkley et al., 1997). The latter approach has been used successfully in a test of the NOAA lidar (Churnside, 1999).

Future application of airborne lidar

An airborne lidar survey could provide a census of epipelagic fishes an order of magnitude faster than that provided by ships, thus reducing costs in dollars (based on 1999 dollar amounts) from about \$100 per ship-survey mile to \$3 per aerial-survey mile (research ship cost=\$12,000 per day, net ship speed including stopping at stations=5 kn; airplane=\$600 per hour at 200 kn).

Faster surveys not only cost less but improve accuracy because steady state assumptions are reduced, vessel avoidance is eliminated, and, most important, high speed makes it practical to survey a much larger area, thereby eliminating the errors associated with partial coverage. No major technical barrier exists in acquiring a suitable instrument; adequate fish detection lidars already exist. Fish-detecting lidars may be purchased from one or more vendors or a radiometric lidar may be assembled from "off the shelf" components as has been done with the NOAA lidar (Churnside and Hunter, 1996). However, to implement routine surveys, signal-processing algorithms for rapid quantification of targets are needed, and if the fish targets are to be converted to biomass, direct calibrations of target strength will be needed.

The depth limitation of lidar is not a major barrier to implementation. Our analysis demonstrates, as does our practical experience, that school detection depths of 30–40 m can be expected for California coastal waters using off-the-shelf instrumentation. In fact, more powerful systems are unlikely to do much better owing to the rapid attenuation of signal with depth. The 30–40 m depth limitation is less important at night because most epipelagic fish schools are found within the volume of water that is to be detected by lidar. Our analysis demonstrated that schools can be detected at night despite a much lower packing density. To deal most effectively with the fraction of undetected schools, survey design should be based on line transect theory and should require an estimate of the average vertical distribution of schools under the specific survey conditions (region, species, season, time of day).

In conclusion, the census of epipelagic fish schools with airborne lidar would be practical and useful today if three conditions could be met: assumptions regarding species identity are acceptable; a line transect survey design is used in conjunction with

the known vertical distribution of schools; and algorithms are developed to process the data.

Acknowledgments

We thank Edgeworth Wester and Wynn Eberhard of Environmental Technology Laboratory, Boulder, Colorado, for reading an early draft, and two anonymous reviewers for their constructive comments and suggestions that improved the presentation of the manuscript. Partial support for J. Churnside was provided by the Advanced Sensor Applications Program of the U.S. Department of Defense.

Literature cited

- Aoki, I., and T. Inagaki.**
1988. Photographic observations on the behaviour of Japanese anchovy *Engraulis japonica* during the night in the sea. *Mar. Ecol. Prog. Ser.* 43:213–221.
- Baxter, J. H. S., and J. R. Hunter.**
1982. The biology of the clupeoid fishes. *In* Advances in marine biology, p. 1–223. Academic Press, New York, NY.
- Buckland, S. T., D. R. Anderson, K. P. Burnham, and J. L. Laake.**
1993. Distance sampling: estimating abundance of biological populations. Chapman and Hall, London, 446 p.
- Castillo Valderrama, P. R.**
1995. Distribucion de los principales recursos pelagicos durante los veranos de 1992 a 1994. Instituto Del Mar Del Peru Informe 114:17–18.
- Checkley, D. M., P. B. Ortner, L. R. Settle, and S. R. Cummings.**
1997. A continuous, underway fish egg sampler. *Fish. Oceanogr.* 6(2):58–73.
- Churnside, J. H.**
1999. Can we see fish from an airplane? *In* Airborne and in-water underwater imaging (Gary D. Gilbert, ed.), p. 45–48. Proc. SPIE (Society of Photo-Optical Instrumentation Engineers) 3761. SPIE, Bellingham, WA.
- Churnside, J. H., and J. R. Hunter.**
1996. Laser remote sensing of epipelagic fishes. *In* Laser remote sensing of natural waters: from theory to practice (V. I. Feigels and Y. I. Kopilevich, eds.), p. 38–53. SPIE, Bellingham, WA.
- Churnside, J. H., J. J. Wilson, and V. V. Tatarskii.**
1997. Lidar profiles of fish schools. *Appl. Opt.* 36:6011–6020.
- Cram, D. L., and I. Hampton.**
1976. A proposed aerial/acoustic strategy for pelagic fish stock assessment. *J. Const. Int. Explor. Mer* 37(1):91–97.
- Feigels, V. I., and Yu. I. Kopilevich.**
1994. Applicability of lidar remote sensing methods for vertical structure investigation of ocean optical properties distribution. *In* Ocean optics XII (J. Jaffe, ed.), p. 449–457. Proc. SPIE 2258.
- Fiedler, P. C.**
1978. The precision of simulated transect surveys of northern anchovy, *Engraulis mordax*, school groups. *Fish. Bull.* 76(3):679–685.
- Gordon, H. R.**
1982. Interpretation of airborne oceanic lidar: effects of multiple scattering. *Appl. Opt.* 21:2996–3001.
- Graves, J.**
1977. Photographic method for measuring spacing and density within pelagic fish schools at sea. *Fish. Bull.* 75:230–234.
- Gunderson, D. R.**
1993. Surveys of fisheries resources. John Wiley and Sons, Inc., New York, NY, 248 p.
- Hara, I.**
1990. Comparison of ship and aerial surveys of sardine schools. *IEEE (Institute of Electrical and Electronic Engineers) Trans. Geosci. Remote Sens.* 28(4):693–695.
- Holliday D. V., and H. L. Larsen.**
1979. Thickness and depth distributions of some epipelagic fish schools off southern California. *Fish. Bull.* 77(2):489–494.
- Hunter, J., and R. Nicholl.**
1985. Visual threshold for schooling in northern anchovy *Engraulis mordax*. *Fish. Bull.* 83(3):235–242.
- Jacobson, L. D., N. C. H. Lo, and J. T. Barnes.**
1994. A biomass-based assessment model for northern anchovy, *Engraulis mordax*. *Fish. Bull.* 92:711–724.
- Jerlov, N. G.**
1968. Optical oceanography. Elsevier, Amsterdam, 194 p.
- Lo, N. C. H., I. D. Jacobson, and J. L. Squire.**
1992. Indices of relative abundance from fish spotter data based on delta-lognormal models. *Can. J. Fish. Aquat. Sci.* 49:2515–2526.
- Mais, K. F.**
1974. Pelagic fish surveys in the California Current. *Calif. Dep. Fish Game, Fish. Bull.* 162, 79 p.
- Misund, O. A.**
1993. Dynamics of moving masses: variability in packing density, shape, and size among herring, sprat, and saithe schools. *ICES J. Mar. Sci.* 50:145–160.
- Mobley, C. D.**
1995. The optical properties of sea water. *In* Handbook of optics, second ed., vol.1, chap. 43 (M. Bass, ed.), p. 36. McGraw-Hill, New York, NY.
- Nakashima, B. S.**
1990. Capelin school surface area index for NAFO Div. 3L during the 1989 spawning season. Northwest Atlantic Fisheries Organization (NAFO) SCR Doc. 90/59, serial no. N1780.
- Petzhold, T. J.**
1972. Volume scattering functions for selected ocean waters. SIO (Scripps Institution of Oceanography) Ref. Doc. 72-78. Scripps Inst. Oceanogr., La Jolla, CA, 82 p.
- Pommeranz, T., and H. G. Moser.**
1987. Data report on the vertical distribution of the eggs and larvae of northern anchovy, *Engraulis mordax*, at two stations in the Southern California Bight March–April 1980. U.S. Dep. Commer., NOAA Tech. Memo. NOAA-TM-NMFS-SWFC-75, 140 p.
- Smith, P. E.**
1981. Fisheries on coastal pelagic schooling fish. *In* Marine fish larvae: morphology, ecology and relation to fisheries (R. Lasker, ed.), 1–31 p. Washington Sea Grant Program, Univ. Washington Press, Seattle, WA.
- Squire, J. L., Jr.**
1972. Apparent abundance of some pelagic marine fishes off the southern and central California coast as surveyed by an airborne monitoring program. *Fish. Bull.* 70:1005–1019.
- Whitney, R. R.**
1969. Schooling of fishes relative to available light. *Tran. Am. Fish. Soc.* 98(3):497–504.

Appendix

The detection probability by depth ($p_a(z)$) was defined as the proportion by which the mean values of SNR_z exceed the threshold, TNR (Eq. 16). Strictly speaking, one should define the detection probability as the expected probability that each signal exceeds the threshold. The expectation would be computed by integrating over the pdf of mean SNR_z . For a lognormal distribution of mean SNR_z , we would have

$$\begin{aligned} P_a(z) &= \int P(s > TNR | SNR_z) \text{lognormal}(SNR_z) dSNR_z \\ &= \int_0^{\infty} [1 - \Phi(TNR - SNR_z)] \frac{1}{\sqrt{2\pi\sigma SNR_z}} \end{aligned}$$

$$\exp\left(-0.5\left(\frac{\ln(SNR_z) - \mu_z}{\sigma}\right)^2\right) d(SNR_z), \quad (20)$$

where s = the signal-noise-ratio which follows normal ($SNR_z, 1$); and SNR_z = a lognormal random variable with mean $\mu_z = \ln(A) + E(\ln(x)) - 2\alpha z$; and standard deviation $\sigma = SD(\ln(x))$ where x is the packing density.

Our exercise indicated that both detection probabilities from Equations 16 and 20 were very similar. Equation 16, although an approximation, was used in our computation because of its simplicity.